Roughness Evolution of Ion Sputtered Rotating InP Surfaces: Pattern Formation and Scaling Laws

F. Frost,* A. Schindler, and F. Bigl

Institut für Oberflächenmodifizierung, Permoserstrasse 15, D-04318 Leipzig, Germany
(Received 24 January 2000)

The topography evolution of simultaneously rotated and Ar$^+$ ion sputtered InP surfaces was studied using scanning force microscopy. For certain sputter conditions, the formation of a highly regular hexagonal pattern of close-packed mounds was observed with a characteristic spatial wavelength which increases with sputter time t according to $\lambda \sim t^\gamma$ with $\gamma \simeq 0.26$. Based on the analysis of the dynamic scaling behavior of the surface roughness, the evolution of the surface topography will be discussed within the limits of existing models for surface erosion by ion sputtering.

Ion bombardment of surfaces is an integral part of many surface processing techniques, including ion sputter etching and deposition, sputter cleaning, ion beam assisted deposition, and reactive ion (beam) etching. These processes often result in a pronounced topography evolution, generally accomplished by a kinetic roughening of the surface. Under special circumstances, i.e., generally for off-normal ion incidence, a periodic height modulation in the form of ripples or wavelike structure with a submicron length scale develops during ion bombardment as observed for single crystalline semiconductor materials (Si [1–6]; Ge [7]; AIII/BVs [8–10]), single crystalline metals (Cu [11,12] and Ag [13]), amorphous materials (SiO$_2$ [14]), and others (e.g., graphite [15]).

Simultaneously, theoretical models have been developed in recent years. Within the Bradley-Harper (BH) model, the origin of this ripple formation can be traced to a surface instability caused by the competition between roughening (curvature dependent sputtering also termed as negative surface tension) and smoothing (surface diffusion also termed as positive surface tension) processes [16]. The resulting ripple orientation (parallel or perpendicular to the projection of the incident ion beam) depends on the incidence angle of the ion beam and the ripple wavelength is given by the ratio between positive and negative surface tension. Refined theories are based on the BH model and include nonlinear effects and noise and describe the time evolution of the surface topography $h(\mathbf{r}, t)$ by means of a stochastic nonlinear continuum equation termed the Kuramoto-Sivashinsky (KS) equation [17–20]. Common to all these experimental and theoretical studies on ripple formation is a preferred direction (anisotropy) of the topography evolution due to the oblique incidence of the ion beam or due to anisotropic surface diffusion.

Among the III-V compound semiconductors, InP is known for an extraordinary roughness development during sputtering. Therefore, the accompanied topography evolution under oblique ion incidence has been studied intensely [9,10,21]; however, no detailed studies have been published on the kinetic roughening of simultaneously rotated and sputtered surfaces. To fill this gap we have studied the topography evolution of simultaneously rotated and low energy Ar$^+$ ion sputtered InP surfaces, as well as the resulting scaling properties. In particular, it is the goal of this study to show that also sputtering of *rotating* InP surfaces generates a highly periodic surface profile, i.e., hexagonal ordered arrays of cones or mounds with dimension less than 100 nm. Based on the determined scaling laws of the surface roughness the evolution of the surface topography will be discussed within the limits of existing models for surface erosion by ion sputtering.

All experiments were performed in a custom-built ion beam etching system with a rotatable substrate stage (for details, see, e.g., Ref. [22]). For the majority of the studies the sample temperature was maintained at 285 K. The samples used in this work were commercially available epi-polished semi-insulating (100) InP substrates characterized by a root-mean-square (rms) roughness $\sigma \simeq 0.2$ nm. The surface topography was investigated by atomic force microscopy (AFM) using a NanoScope III from Digital Instruments. All measurements were conducted in air using silicon tips with a nominal tip radius of <10 nm [23]. The results presented were extracted from over 1500 AFM measurements of more than 170 samples exposed to total ion doses between 3.75×10^{15} and 9.0×10^{18} cm^{-2}.

In Fig. 1 we report AFM images from InP surfaces simultaneously rotated and sputtered at an incidence angle $\alpha_{\text{ion}} = 40°$ (with respect to the surface normal), an ion energy $E_{\text{ion}} = 500$ eV, an ion flux $j_{\text{ion}} = 150 \ \mu\text{A cm}^{-2}$, and different times t (ion doses). Immediately after the start of sputtering moundlike or conelike structures begin to appear [Fig. 1(a)]; their lateral size and height become larger as the sputtering proceeds [Fig. 1(b)]. For longer sputter times, the lateral size (or spatial wavelength) of the mounds saturates and the topography changes from a more irregular to a highly regular hexagonal pattern of mounds [Fig. 1(c)]. In order to clarify this pattern formation the two-dimensional autocorrelation function $C(\mathbf{r}, t) = \langle h(\mathbf{r}, t) h(0, t) \rangle$ (where $\langle \rangle$ denotes the spatial
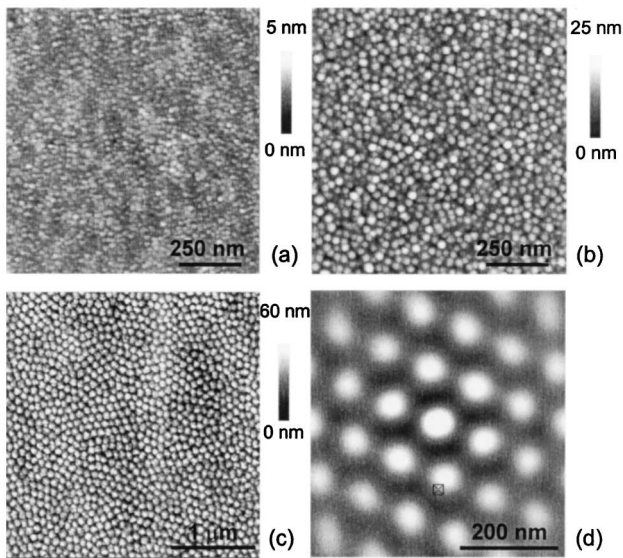
FIG. 1.   AFM images, showing a sequence of the evolution of InP surface topography with increasing sputter time t (ion dose) at $t = 10$ s (a), $t = 40$ s (b), and $t = 9600$ s (c). The ion beam parameters were Ar^+ ion energy 500 eV, incidence angle 40°, ion current density 150 $\mu A\,cm^{-2}$. Image (d) represents the two-dimensional autocorrelation function calculated from a magnified area of image (c) which clearly shows the hexagonal symmetry of the mound arrangement. The lateral size of the images are 1 μm for (a) and (b), 3 μm (c), and 500 nm (d), respectively.

FIG. 2.   AFM images (scan size 3 μm) of Ar^+ sputtered InP surfaces ($E_{ion} = 500$ eV, $j_{ion} = 150$ $\mu A\,cm^{-2}$, $t = 1200$ s) at an incidence angle of $\alpha_{ion} = 10°$ (a), $\alpha_{ion} = 30°$ (b), $\alpha_{ion} = 70°$ (c), and $\alpha_{ion} = 80°$ (d).

average) from a magnified area of image (c) was calculated and shown in Fig. 1(d). The wavelength of the mounds was given by $\lambda = (84 \pm 5)$ nm, determined either from the autocorrelation function or alternatively from the circularly averaged power spectra. An inspection of the mound structures using high-resolution transmission electron microscopy reveals that the mounds have the same atomic structure as the InP bulk material. It should be noted that without sample rotation the surface topography is decisively different; i.e., the overall roughness is much higher as with rotation. Furthermore, the observed conelike structures are oriented toward the direction of the ion beam incidence in accordance with other studies [9,21]. Although the resulting overhangs in the height profile make a quantitative evaluation of the AFM images very difficult, no evidence for the formation of periodic surface structure was found.

Next, we will answer the question about which parameters control the surface evolution. In Fig. 2 a sequence of sputtered surfaces at different incidence angles of the ion beam ($E_{ion} = 500$ eV, $j_{ion} = 150$ $\mu A\,cm^{-2}$, $t = 1200$ s) was shown. Up to $\alpha_{ion} \lesssim 50°$ [Figs. 2(a) and 2(b)] the close-packed hexagonal mound pattern is conserved; for further increasing of α_{ion} the periodic pattern vanishes [Fig. 2(c)]. Last, at $\alpha_{ion} = 80°$ mound formation again appears [Fig. 2(d)], but with a smaller mound size as for $\alpha_{ion} \lesssim 50°$. The functional dependence of the rms surface roughness σ and the spatial wavelength λ on
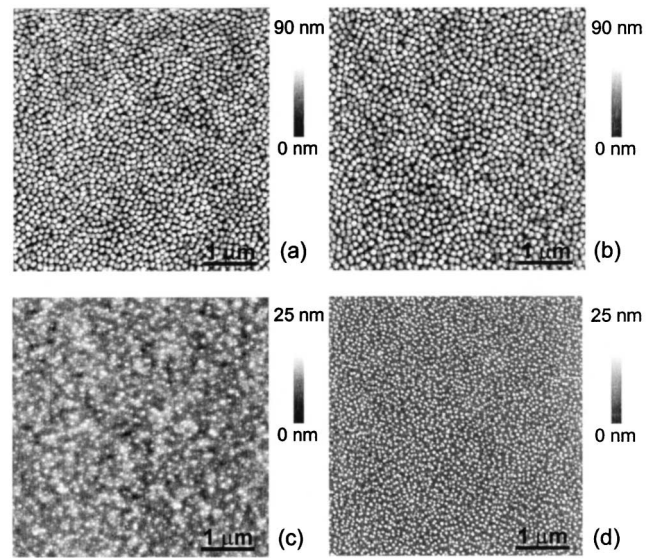
α_{ion} are summarized in Fig. 3. In addition, the dependence of the surface topography on ion energy was examined (for fixed $\alpha_{ion} = 40°$, $200 \leq E_{ion} \leq 1200$ eV). Pattern formation could be observed for all ion energies $E_{ion} \gtrsim 350$ eV, whereas σ as well as λ increase with increasing ion energy. Besides the above-named parameters also the sample temperature is critical for the evolution of the topography. Within the investigated temperature range ($T_S = 285-375$ K) both σ and λ increase with T_S. Specifically, at temperatures $T_S > 315$ K the formation of hexagonal ordered arrays is almost lost. A more detailed description of the evolution of the surface with respect to sputter parameters will be given elsewhere.

In order to gain insight into the detailed sputter processes and the scaling behavior, the roughness exponent α and the growth exponent β were determined. According to the scaling theory [24] these quantities are given by the temporal and spatial scaling of the rms surface roughness $\sigma = \sqrt{\langle [h(\mathbf{r}, t) - \langle h(\mathbf{r}, t) \rangle]^2 \rangle}$ following the relation $\sigma(L, t) \sim L^\alpha f(t/L^{\alpha/\beta})$ [where L is the system size, $f(u) \sim u^\beta$ for $u \ll 1$, and $f(u \to \infty) \sim$ const], respectively. The value of β was extracted from a linear fit of the log-log plot of σ vs t. The exponent α was determined from a fit to the linear part of the log-log plot of $H(r, t)^{1/2}$ vs r, where $H(r, t)$ is the height-height correlation function given by $H(r, t) = \langle [h(r, t) - h(0, t)]^2 \rangle$ (cf. Ref. [24]). The results as a function of sputter time ($\alpha_{ion} = 40°$, $E_{ion} = 500$ eV, $j_{ion} = 150$ $\mu A\,cm^{-2}$) are shown in Fig. 4, together with the time scaling behavior of the mound wavelength $\lambda \sim t^\gamma$. Clearly, we can recognize a crossover in the power law scaling of $\sigma(t)$ from $\beta = 0.80 \pm 0.10$ in the early-time regime to $\beta = 0.27 \pm 0.06$ in the late-time regime. In contrast, within the error margin, the
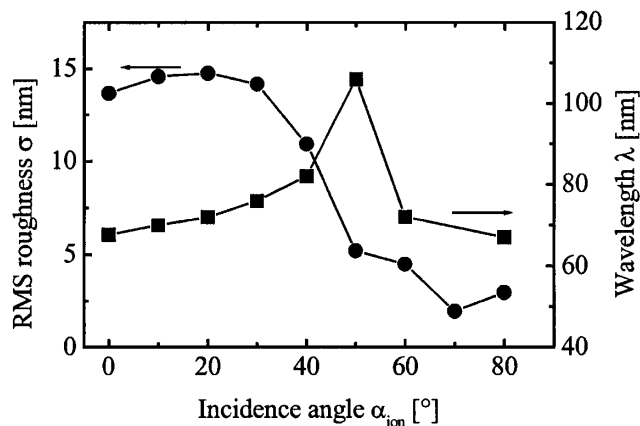
FIG. 3. Dependence of the rms surface roughness σ and the spatial wavelength λ on the ion incidence angle α_{ion} ($E_{ion} = 500$ eV, $j_{ion} = 150$ $\mu A\,cm^{-2}$, $t = 1200$ s).

value of $\alpha = 0.7-0.8$ was nearly time invariant. Further, the spatial wavelength of the mounds underlies a coarsening process with $\gamma = 0.26 \pm 0.04$. Similar scaling laws could be found for sputtering at other ion fluxes and incidence angles. For instance, at $\alpha_{ion} = 0°$, $E_{ion} = 500$ eV, and $j_{ion} = 150$ $\mu A\,cm^{-2}$ we found $\beta = 0.91 \pm 0.14$, $\beta = 0.33 \pm 0.05$ (after crossover), $\alpha = 0.7-0.8$, and $\gamma = 0.30 \pm 0.04$.

How can we understand the observed scaling behavior within the existing models for surface erosion by ion sputtering? Recently, Bradley has shown that the evolution of the surface for sufficient fast rotating samples can be described by a modified version of the KS equation [25,26]. In order to enlighten the behavior of the KS equation, Drotar *et al.* [27] performed a numerical simulation in $2 + 1$ dimensions. In accordance with simulations in $1 + 1$ dimensions by Cuerno *et al.* [18], they observed mainly three time regimes with different values of β, but a nearly time-invariant $\alpha = 0.7-0.8$. If we assume that their very early-time regime is not accessible within our experiments [28] then our findings for α and β roughly correspond to the results of the simulations. Consequently, it might be concluded that the time evolution of the surface topography is reasonably described by the use of the KS equation. However, there are several experimental findings that are not consistent with the KS equation or the BH model.

Although an increasing mound size λ at higher temperatures T_S is predicted by the BH model no quantitative match between the observed $\lambda(T_S)$ behavior and the BH model was found. Another open question is the mechanism that underlies the mound coarsening process $\lambda \sim t^\gamma$ which is not consistent with the KS equation. Recently, a ripple and mound coarsening with $\gamma \simeq 0.26$ and $\gamma \simeq 0.27$ was detected for Ar^+ sputtering of Cu [11] and Au [29] surfaces, respectively. Both observations were attributed to a Schwoebel barrier for the interlayer diffusion. To what extent is this mechanism also applicable in the present case? Normally, it is reasonable to suppose that for sputtering on InP a diffusion bias or a Schwoebel barrier should have only minor importance due to the amorphization of the
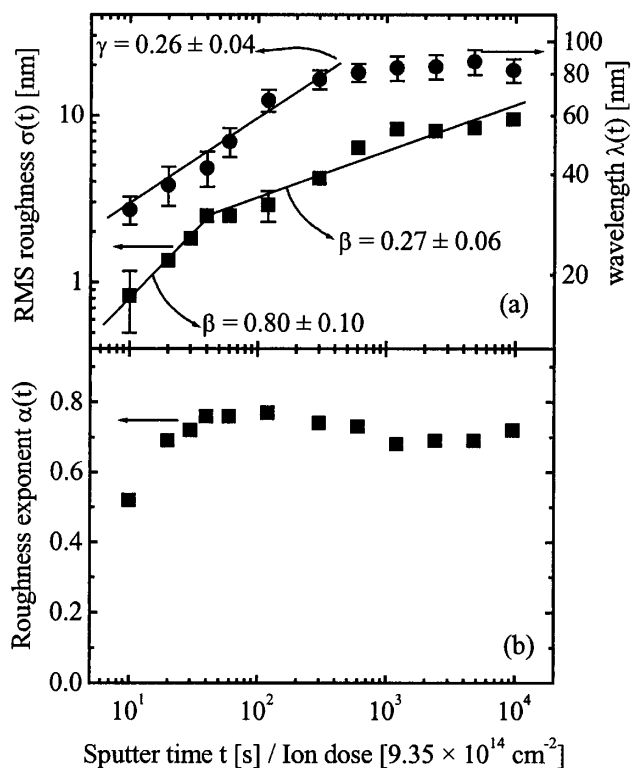

FIG. 4. (a) Mound wavelength λ, rms surface roughness σ, and (b) roughness exponent α vs sputter time t (equivalent ion dose) for sputtering at $E_{ion} = 500$ eV, $\alpha_{ion} = 40°$, and $j_{ion} = 150$ $\mu A\,cm^{-2}$. The error bars plotted for σ vs t correspond to the standard deviation obtained from five experimental runs, whereas σ was estimated from more than 50 AFM images. The other displayed values represent the average over two experimental runs.

near surface region during sputtering. Typically, the amorphization dose is $\lesssim 3 \times 10^{15}$ cm^{-2} with an amorphization depth up to 6 nm for the ion energies considered above [30]. However, it is an established fact for Ar^+ sputtering of nonrotating InP surfaces under oblique ion incidence that excess In atoms are produced by preferential sputtering of P atoms. Because of an enhanced diffusion these In atoms agglomerated into In islands [8,21]. Enforced by the bombardment with energetic ions the In islands can be converted into small In crystallites whereby the growth process is nearly epitaxial [21]. Because the sputter rates for In and InP are different the In agglomerates act as seeding points for the ongoing cone formation by sputtering. Therefore it is perfectly possible that a Schwoebel barrier affects the topography evolution in the early times of sputtering.

Additionally, we should consider a further mechanism responsible for the observed mound coarsening. Caused by the preferential loss of P the enrichment and agglomeration of In result in spatial varying concentrations of In adatoms at the surface. Recently, Mayr *et al.* [31] have evidenced that a diffusion current driven by a concentration gradient of the adatoms is able to generate a structure or mound coarsening. In order to simulate this concentration-gradient-triggered diffusion in the vapor

deposition of amorphous ZrAlCu films they added the nonlinear term $C/2\nabla^2(\nabla h)^2$ with $C > 0$ to the continuum growth equation $\partial h/\partial t = -D\nabla^4 h - S\nabla^2 h + \eta(\vec{r}, t)$ that include surface diffusion ($D > 0$) and the curvature dependent deposition processes ($S > 0$). Numerical simulations in the $1 + 1$ dimension showed, in addition to the coarsening effect, scaling exponents similar to the exponents obtained in the analysis of the KS equation. This is noteworthy, but, from a simplified point of view, not surprising because both equations are identical if we neglect the nonlinear terms and, furthermore, both nonlinear terms have a comparable effect, namely, they hinder the runaway growth of the unstable mode, given by the balance between the two linear terms. Returning to our scaling results for sputtering of InP we can conclude that In enrichment and agglomeration are the main mechanisms for the observed mound coarsening in the initial stage of sputtering. After passing this stage, the topography evolution is mainly described by the KS equation. The aforementioned discussion implicates that especially for the surface topography evolution of compound materials additional processes, e.g., caused by concentration gradients at the surfaces, should be considered for a more complete description of the surface topography evolution during sputter erosion.

In summary, we have demonstrated that ion sputtering of rotating InP surfaces under oblique incidence causes the formation of a highly hexagonally ordered close-packed array of cones or mounds with dimensions less than 100 nm which offers a lot of potential applications in the field of nanotechnology [32]. The scaling laws of the surface roughness were only partially consistent with predictions of the KS equation, especially in the initial stage of sputtering where processes that are characteristic for compound materials must be taken into account.

---

*Electronic mail: ffrost@server1.rz.uni-leipzig.de

[1] G. Carter, M. J. Nobes, F. Paton, and J. S. Williams, Radiat. Eff. **33**, 65 (1977).

[2] K. Elst, W. Vandervorst, J. Alay, J. Snauwaert, and L. Hellemans, J. Vac. Sci. Technol. B **11**, 1968 (1993).

[3] G. Carter and V. Vishnyakov, Phys. Rev. B **54**, 17 647 (1996).

[4] J. J. Vajo, R. E. Doty, and E.-H. Cirlin, J. Vac. Sci. Technol. A **14**, 2709 (1996).

[5] Z. X. Jiang and P. F. A. Alkemade, Appl. Phys. Lett. **73**, 315 (1998).

[6] J. Erlebacher, M. J. Aziz, E. Chason, M. B. Sinclair, and J. A. Floro, Phys. Rev. Lett. **82**, 2330 (1999).

[7] E. Chason, T. M. Mayer, B. K. Kellerman, D. T. McIlroy, and A. J. Howard, Phys. Rev. Lett. **72**, 3040 (1994).

[8] S. W. MacLaren, J. E. Baker, N. L. Finnegan, and C. M. Loxton, J. Vac. Sci. Technol. A **10**, 468 (1992).

[9] J. B. Malherbe, CRC Crit. Rev. Solid State Mater. Sci. **19**, 55 (1994), and references therein.

[10] C. M. Demanet et al., Surf. Interface Anal. **23**, 433 (1995); **24**, 497 (1996); **24**, 503 (1996).

[11] S. Rusponi, G. Costantini, C. Boragno, and U. Valbusa, Phys. Rev. Lett. **81**, 4184 (1998).

[12] S. Rusponi, G. Costantini, C. Boragno, and U. Valbusa, Phys. Rev. Lett. **81**, 2735 (1998).

[13] S. Rusponi, C. Boragno, and U. Valbusa, Phys. Rev. Lett. **78**, 2795 (1997).

[14] T. M. Mayer, E. Chason, and A. J. Howard, J. Appl. Phys. **76**, 1633 (1994).

[15] S. Habenicht, W. Bolse, K. P. Lieb, K. Reimann, and U. Geyer, Phys. Rev. B **60**, R2200 (1999).

[16] R. M. Bradley and J. M. E. Harper, J. Vac. Sci. Technol. A **6**, 2390 (1988).

[17] R. Cuerno and A.-L. Barabási, Phys. Rev. Lett. **74**, 4746 (1995).

[18] R. Cuerno, H. A. Makse, S. Tomassone, S. T. Harrington, and A.-L. Barabási, Phys. Rev. Lett. **75**, 4464 (1995).

[19] K. B. Lauritsen, R. Cuerno, and H. A. Makse, Phys. Rev. E **54**, 3577 (1996).

[20] M. Rost and J. Krug, Phys. Rev. Lett. **75**, 3894 (1995).

[21] M. Nozu, M. Tanemura, and F. Okuyama, Surf. Sci. Lett. **304**, L468 (1994).

[22] F. Frost, G. Lippold, A. Schindler, and F. Bigl, J. Appl. Phys. **85**, 8378 (1999).

[23] In order to achieve a reproducible tip radius and, consequently, minimize tip convolution effects each tip undergoes a special calibration procedure. For this procedure we used samples sputtered less than 20 s and demanded that the minimal lateral dimension of the observed surface features should be ≤ 10 nm.

[24] A.-L. Barabási and H. E. Stanley, *Fractal Concepts in Surface Growth* (Cambridge University Press, Cambridge, England, 1995).

[25] R. M. Bradley, Phys. Rev. E **54**, 6149 (1996).

[26] R. M. Bradley and E.-H. Cirlin, Appl. Phys. Lett. **68**, 3722 (1996).

[27] J. T. Drotar, Y.-P. Zhao, T.-M. Lu, and G.-C. Wang, Phys. Rev. E **59**, 177 (1999).

[28] The very early stage of sputtering in our experiments remains an open question because the smallest reproducible adjustable sputter time was 10 s.

[29] M. V. Ramana Murty, T. Curcic, A. Judy, B. H. Cooper, A. R. Woll, J. D. Brock, S. Kycia, and R. L. Headrick, Phys. Rev. Lett. **80**, 4713 (1998).

[30] H. Gnaser, in *Low-Energy Ion Irradiation of Solid Surfaces*, edited by G. Höhler, Springer Tracts in Modern Physics Vol. 146 (Springer, Berlin, Heidelberg, New York, 1999), p. 184.

[31] S. G. Mayr, M. Moske, and K. Samwer, Phys. Rev. B **60**, 16 950 (1999).

[32] Concurrent in time with our investigations, S. Facsko et al. discovered accidentally a special case of the observed pattern formation process, namely, Ar^+ ion sputtering of GaSb at $\alpha_{ion} = 0°$, and they exploit this process to generate a regular array of quantum dots in GaSb [Science **285**, 1551 (1999)].